IEEE Access
Multidisciplinary | Rapid Review | Open Access Journal

Received March 2, 2019, accepted March 21, 2019, date of publication April 1, 2019, date of current version April 17, 2019.

Digital Object Identifier 10.1109/ACCESS.2019.2908383

Robust Current Controller for IPMSM Drives Based on Explicit Model Predictive Control With Online Disturbance Observer

CHENGYU JIA[1], XUDONG WANG[1], YAFEI LIANG[2], AND KAI ZHOU[1]
[1]School of Electrical and Electronic Engineering, Harbin University of Science and Technology, Harbin 150080, China
[2]Motor Technologies (Beijing) Co., Ltd., Beijing 100176, China

Corresponding author: Chengyu Jia (chengyujia@163.com)

This work was supported in part by the University Nursing Program for Young Scholars with Creative Talents in Heilongjiang Province, under Grant UNPYSCT-2017099.

ABSTRACT To improve the performance of a current loop, this paper presents a novel current control scheme for an interior permanent magnet synchronous motor (IPMSM) based on the model predictive control (MPC) algorithm in a synchronous rotating frame (dq-frame). The recently developed explicit MPC (EMPC) is introduced to ensure the feasibility of real-time implementation in the control hardware. To achieve feasible reformulation of the current control problem using EMPC, a coupled nonlinear IPMSM mathematical model is linearized using an augmented model with disturbance. Furthermore, to approximate the related quadratic stator current and voltage constraints in the dq-frame, they are also transformed into a series of linear inequalities. We propose an improved disturbance observer based on the augmented model, in conjunction with the concept of offset-free MPC, to estimate both the disturbance terms and the state variables from the predicted and measured outputs. All the influences of plant/model mismatches and un-modeled nonlinear terms are removed by the estimated total disturbance within the closed-loop framework of EMPC. The proposed EMPC scheme not only improves both the dynamic performance and the steady-state precision of the current loop, but it also exhibits robustness against parameter uncertainties. The proposed method has been proven and verified successfully in both simulation and experiment.

INDEX TERMS Interior permanent magnet synchronous motor (IPMSM), current control, model predictive control (MPC), explicit solution, disturbance observer.

I. INTRODUCTION

Interior permanent magnet synchronous motors (IPMSMs) are characterized by strong reliability, high power density, high efficiency, and a large torque–ampere ratio. Therefore, IPMSMs are used extensively in the automotive industry as traction motors [1]. For IPMSM drive control in electric vehicle and hybrid electric vehicle applications, improving both the dynamic and the steady-state current control performance is essential for smooth driving, energy saving, good vibration behavior, and noise control of the vehicle. Furthermore, because of safety considerations, there are strict limitations on the operation of IPMSMs, e.g., the maximum allowable stator current magnitude and maximum achievable voltage of the voltage source inverter. A widely adopted current control method for an automotive traction motor is the single-input single-output proportional-integral (PI) controller with a feedforward cross-coupling compensation method based on field-oriented control [2]. The PI controller is used most commonly in practice because it has good disturbance rejection properties, and it is insensitive to system parameter variation. However, PI control does not have an optimal dynamic response because of the reasonably low transient response of the integral components. In a PI controller, the system constraints are considered by saturation of the corresponding values and anti-windup in case of actuating value saturation to suppress output overshooting. Anti-windup also leads to an imperfect dynamic response [3]. In attempts to both overcome these shortcomings and improve the performance of current tracking, various current control techniques have been introduced, such as internal model control [4], fuzzy control [5], sliding mode control [6], neural network inverse

The associate editor coordinating the review of this manuscript and approving it for publication was Xiaodong Sun.

method [7] and [8], and model predictive control (MPC) [9] and [10]. Among these algorithms, MPC is proposed as a feasible alternative for current control of electric machines because of its fast dynamic performance and multivariable constraint control capability [11]. MPC uses a mathematical model of the system with measured states to predict the future behavior of the controlled variables. The prediction results are evaluated using a customized cost function based on the difference between the actual output and the trajectory to be tracked. MPC casts the control problem as an optimization problem, which makes it convenient for handling constraints and nonlinear models explicitly. The optimal state–space control problem is solved at each time step, which provides the control action sequence. The asymptotic stability and the optimality of constrained MPC are discussed in [12]. Compared with other control methods, the main advantage of MPC is that the safety and physical limitations of a drive can be incorporated as control objectives directly into the control problem formulation such that future constraint violations can be anticipated and prevented.

Despite the abovementioned advantages, the real-time implementation of MPC brings high computational burden because of the finite-horizon optimal control problem solved at each sampling period. To reduce the amount of online computation, some researchers [13] introduced an explicit solution of constrained MPC, i.e., the so-called explicit MPC (EMPC). EMPC can achieve the same performance as MPC and it inherits the stability of MPC. With this concept, the optimization problem can be solved offline, and the controller can be depicted by piecewise affine (PWA) functions [14], which significantly reduces the online computational burden, making it suitable for real-time implementation with fast sampling rates. An EMPC-based design is given in [15], where a combination of speed and current control in a single controller was applied to an electromechanical model of a permanent magnet synchronous motor (PMSM) in a synchronous rotating frame (dq-frame). To deal with the problem of unmeasured disturbance, an extra integrator was superimposed on the MPC to remove the steady-state error. A PMSM control method [16] was developed based on EMPC using a novel linearization and constraint handling method, which allowed natural field weakening. It also added an extra compensation voltage calculation to the controller output to remove the inaccuracy introduced by the model linearization process.

Another disadvantage of using MPC is that its performance depends largely on the accuracy of the model. Furthermore, the effects of un-modeled nonlinear disturbances and plant/model mismatch cause that the output prediction error must to be considered during the MPC design. Several articles addressing this problem have been published. For example, some researchers [17] presented a method for a design of an integrated disturbance model and observer to achieve offset-free MPC. Others [18] reviewed the main approaches proposed for achieving offset-free control. In addition, results that were more generalized were derived [19], which presented the conditions that ensured detectability of the augmented system. A theoretical analysis of the offset-free properties of such an augmentation, within the MPC framework was performed [20]. An EMPC design for a current loop with estimation of the disturbances using the recursive least squares method fed forward for compensation was discussed [21]. An EMPC speed controller for an induction machine was designed considering load disturbance as an additional state variable, and a Kalman filter was applied to correct the predicted state variables to reject the disturbance [22]. A state and disturbance observer was designed based on a quadratic Lyapunov function, as proposed in another study [23], to guarantee asymptotic stability of the estimation error for MPC-based PMSM current control. In summary, most current formulations of MPC/EMPC with disturbance rejection have a disturbance observer, together with a dynamically constrained cost function and a target calculator. The disturbance observer techniques for the estimation of the additional system states, e.g., the Luenberger observer, Kalman filter, or extended Kalman filter, were studied [24]–[26].

Many MPC/EMPC techniques have been successfully applied to PMSM drives in the past. Unfortunately, only a few papers have discussed the application of MPC/EMPC to the current control of IPMSMs. This motivated us to propose an EMPC scheme for application to IPMSMs. The main contribution of this paper is the presentation of a complete procedure for the formulation of an EMPC controller for the IPMSM current control problem. It includes the linearization of the plant, constraint linearization handling, and offset-free control MPC implementation, particularly when designing an adaptive disturbance observer aimed at negation of the effects of plant/model mismatches and un-modeled nonlinear terms. The remainder of this paper is organized as follows. An overview of the basic theoretical background of MPC is presented in Section II. The IPMSM drive model is described in Section III. The EMPC framework design and its implementation are presented in Section IV. Section V provides the results obtained from simulation and experiment. Finally, our conclusions are summarized in Section VI.

II. BACKGROUND OF MODEL PREDICTIVE CONTROL

The principal concept of MPC is to use a model of a plant to predict the future evolution of the system. The most common way to describe a system is to use of a state–space model. For a linear time-invariant (LTI) dynamical system with n state variables, m inputs, and p outputs, the discrete-time state–space formulation at time instant k is given by

$$\begin{cases} x(k+1) = \boldsymbol{A}x(k) + \boldsymbol{B}u(k) \\ y(k) = \boldsymbol{C}x(k) \end{cases} \tag{1}$$

where $x \in \mathbb{R}^n$, $u \in \mathbb{R}^m$, and $y \in \mathbb{R}^p$ are the system state, system input, and output variables, respectively. The system variables are limited by the constraints $u_{\min} \leq u(k) \leq u_{\max}$ and $y_{\min} \leq y(k) \leq y_{\max}$. The model matrices $\boldsymbol{A}$ and $\boldsymbol{B}$ allow

prediction of the evolution of the system as a function of the initial state $x(k)$. For a linear constrained system, the MPC control objective is commonly formulated as a quadratic cost function:

$$J(\boldsymbol{U}, x(k)) = \sum_{i=0}^{N_p} x(k+i)^T \boldsymbol{Q} x(k+i) + \sum_{i=0}^{N_u-1} u(k+i)^T \boldsymbol{R} u(k+i) \quad (2)$$

where $\boldsymbol{U} = [u(k)^T, \ldots, u(k+N_u-1)^T]^T \in \mathbb{R}^{m*N_u}$ is the control input sequence; N_p and N_u are the prediction horizons and control horizons, respectively, with $N_u \leq k < N_p$. The input is supposed to be constant after $N_u + k - 1$; $\boldsymbol{Q}$ and $\boldsymbol{R}$ are symmetric and non-negative defined weighted matrices, penalizing the state and the control input with appropriate weighting factors over the prediction horizon N_p; The control law is computed by solving the following constrained optimal control problem at each time step:

$$\begin{aligned} &\min_{\boldsymbol{U}} \ J(\boldsymbol{U}, x(k)) \\ &s.t. \ x(k+i) = \boldsymbol{A}x(k) + \boldsymbol{B}u(k), \quad i = 1, \ldots, N_p \\ &\quad y(k+i) = \boldsymbol{C}x(k+i), \quad i = 1, \ldots, N_p \\ &\quad u_{\min} \leq u(k+i) \leq u_{\max}, \quad i = 0, \ldots, N_u - 1 \\ &\quad y_{\min} \leq y(k+i) \leq y_{\max}, \quad i = 1, \ldots, N_p \end{aligned} \quad (3)$$

More precisely, the basic principle of MPC can be summarized as follows. At a given sampling instant k, using the current state $x(k)$ as the initial state, the optimization problem (3) yields an open-loop optimal control sequence. Once the optimal control input sequence $\boldsymbol{U}_k^*$ is obtained, only the first control input u_k^* will be applied to the physical system. At sampling instant $k+1$, based on the latest measured value of $x(k+i)$, the new optimal input u_{k+1}^* is obtained for the shifted horizon and subsequently applied. The control scheme updates the state and calculates the optimal control input sequence for the shifted prediction horizon in a receding horizon fashion. This is the main feature of MPC, combining the open-loop optimal control laws and state feedback. By introducing $x(k+i) = A^i x(k) + \sum_{j=0}^{i-1} A^j B u(k+i-1-j)$ into (3), the MPC problem can be solved by quadratic programming (QP):

$$\begin{aligned} J'(\boldsymbol{U}, x(k)) &= \frac{1}{2} x(k)^T \boldsymbol{Y} x(k) + \min_{\boldsymbol{U}} \{\frac{1}{2} \boldsymbol{U}^T \boldsymbol{H} \boldsymbol{U} + x(k)^T \boldsymbol{F} \boldsymbol{U}\} \\ \text{s.t. } \boldsymbol{G}\boldsymbol{U} &\leq \boldsymbol{W} + \boldsymbol{E}x(k) \end{aligned} \quad (4)$$

where $\boldsymbol{H} = \boldsymbol{B}^T \boldsymbol{Q} \boldsymbol{B} + \boldsymbol{R}$, $\boldsymbol{F} = \boldsymbol{A}^T \boldsymbol{Q} \boldsymbol{B}$, and $\boldsymbol{Y} = \boldsymbol{A}^T \boldsymbol{Q} \boldsymbol{A}$. The matrices $\boldsymbol{G}$, $\boldsymbol{W}$, and $\boldsymbol{E}$ can be calculated from $\boldsymbol{Q}$ and $\boldsymbol{R}$ in (2). However, solving the QP problem online involves a high computational burden. To reduce the computational effort, EMPC is introduced in this paper. In EMPC, the state variable $x(k)$ is treated as a parameter vector. By introducing $\boldsymbol{z} = \boldsymbol{U} + \boldsymbol{H}^{-1} \boldsymbol{F}^T x(k)$, we can rewrite the optimization problem (4) as follows:

$$\begin{aligned} J_z'(x(\mathrm{k}), \boldsymbol{U}) &= \min_{z} \frac{1}{2} \boldsymbol{z}^T \boldsymbol{H} \boldsymbol{z} \\ s.t. \ \boldsymbol{G}\boldsymbol{z} &\leq \boldsymbol{W} + \boldsymbol{S}x(k) \end{aligned} \quad (5)$$

with $\boldsymbol{S} = \boldsymbol{E} + \boldsymbol{G}\boldsymbol{H}^{-1}\boldsymbol{F}^T$. In this way, the QP problem turns into a multiparameter programming (mp-QP) problem that can be used to compute its solution offline. The explicit solution defines the optimal control law, which is expressed as a PWA function over a finite number of contiguous regions in the subdivision of feasible states with respect to the parameter vector. In each region of the state space, the PWA control law is expressed as follows:

$$u_i(k) = \boldsymbol{F}_i x(k) + \boldsymbol{G}_i \quad (6)$$

where i is the index of the active region in which the state $x(k)$ is contained at sampling instant k. The matrices $\boldsymbol{F}_i$ and $\boldsymbol{G}_i$ are the results of the optimization algorithm described elsewhere [27]. The optimal control laws are precomputed and read from a lookup table (LUT). The online calculation part is reduced to search the region in which the current state $x(k)$ belongs, and the associated PWA control law can be returned by the active region. This is only a brief description of EMPC; a more detailed explanation is available [13] and [14]. Many efficient algorithms are available for use in searching for control laws, e.g., the binary tree [28]. In particular, the multiparametric toolbox (MPT) [29] of MATLAB can efficiently solve the optimization problems and export the PWA control law stored in a lookup table that can be ported to the target application. Moreover, it also provides routines to generate region partitions and binary search trees for its simulation and implementation.

III. MODELING AN IPMSM

A. MOTOR MODEL

We assumed that all electrical parameters are constant at steady state and ignored iron loss. In the dq-frame with the d-axis fixed to the rotor PM flux linkage vector, the stator current equation of a star-connected three-phase IPMSM is characterized by the following equations:

$$\begin{cases} \dfrac{\mathrm{d}i_d}{dt} = \dfrac{u_d}{L_d} + \dfrac{L_q}{L_d}\omega_e i_q - \dfrac{R_s}{L_d} i_d \\ \dfrac{di_q}{dt} = \dfrac{u_q}{L_q} - \dfrac{L_d}{L_q}\omega_e i_d - \dfrac{R_s}{L_q} i_q - \dfrac{\Psi_f}{L_q}\omega_e \end{cases} \quad (7)$$

where u_d and u_q are the d- and q-axis components of the stator voltage, respectively; ω_e is the rotor electrical speed, which is related to the rotor mechanical speed ω_m by $\omega_e = P_n \omega_\mathrm{m}$, with P_n denoting the number of pole pairs; and i_d and i_q are the d- and q-axis components of the stator current, respectively. Here, d/dt is the differential operator, R_s denotes the stator windings per-phase resistance, L_d and L_q are the d- and q-axis inductances, respectively, and Ψ_f denotes the magnet's flux linkage established by permanent magnets. Because MPC requires a discrete time model, the electrical dynamics of an IPMSM need to be well approximated. To this

end, the forward Euler discretization technique was used to obtain a time-discrete state–space model with time step T_s:

$$\begin{cases} i_d(k+1) = (1 - T_s\frac{R_s}{L_d})i_d(k) + T_s\frac{L_q}{L_d}\omega_e(k)i_q(k) \\ \qquad\qquad + \frac{T_s}{L_d}u_d(k) \\ i_q(k+1) = (1 - T_s\frac{R_s}{L_q})i_q(k) - T_s\frac{L_d}{L_q}\omega_e(k)i_d(k) \\ \qquad\qquad - T_s\frac{\Psi_f}{L_q}\omega_e(k) + \frac{T_s}{L_q}u_q(k) \end{cases} \tag{8}$$

B. MOTOR MODEL LINEARIZATION FOR MPC

Good models for MPC must be descriptive enough to capture the most significant dynamics of the system and simple enough for solving the optimization problem. As mentioned in Section II, the MPC optimization problem represented by the constrained LTI system can be processed offline with minimal complexity. For this reason, a linear system model should be developed, given that the plant model described in (8) is a nonlinear set of equations even if electrical and mechanical parameters are constant, for which the motional coupling terms in each of the equations involves the product of the electrical angular velocity and the current of the other axis. In automotive electric traction drives, the stator phase currents and the rotor position are measured by sensors; thus, i_d and i_q can be obtained using the Clarke and Park transformation sequentially with the measured phase current. The rotor electrical angular velocity can be calculated from the measured rotor position signal. By introducing the auxiliary vector $\boldsymbol{\varsigma}(k) = \left[\varsigma_d(k)\ \varsigma_q(k)\right]^T \in \mathbb{R}^2$, the speed-dependent terms are lumped into this auxiliary vector of the form $\left[\varsigma_d(k)\ \varsigma_q(k)\right]^T = \left[\omega_e(k)L_q i_q(k)\ -\omega_e(k)(L_d i_d(k) + \Psi_f)\right]^T$ in which ω_e is used as a variable parameter as it only varies slowly with the rotor reference frame angular velocities. However, $\boldsymbol{\varsigma}(k)$ contains the time-varying parts at the time instant k. It should be noted that the parametric variation can be considered by using a disturbance observer [19]. Although $\boldsymbol{\varsigma}(k)$ varies quickly during fast current transients, the corresponding evolution of $\boldsymbol{\varsigma}(k)$ can be easily predicted in each current loop control cycle using the disturbance observer. In this way, the auxiliary vector $\boldsymbol{\varsigma}(k)$ is assumed to be a constant disturbance throughout the MPC prediction horizon

$$\boldsymbol{\varsigma}(k+i) = \boldsymbol{\varsigma}(k) \quad i \in \{1 \ldots N_p - 1\} \tag{9}$$

which is updated by an observer at the beginning of the prediction process. During our simulations and experiments, we found that based on assumption (9), we achieved good performance in all operating conditions. Moreover, all the disturbance effects of un-modeled nonlinear terms and plant/model mismatches can also be attributed to $\boldsymbol{\varsigma}(k)$. The linearized discrete-time state–space model of an IPMSM for MPC can be rewritten in the following form:

$$\begin{cases} \boldsymbol{x}(k+1) = \boldsymbol{A}_d\boldsymbol{x}(k) + \boldsymbol{B}_d\boldsymbol{u}(k) + \boldsymbol{B}_\varsigma\boldsymbol{\varsigma}(k) \\ \boldsymbol{y}(k) = \boldsymbol{C}_d\boldsymbol{x}(k) \end{cases} \tag{10}$$

where $\boldsymbol{x}(k) = [i_d(k)i_q(k)]^T \in \mathbb{R}^2$, $\boldsymbol{u}(k) = [u_d(k)u_q(k)]^T \in \mathbb{R}^2$, and $\boldsymbol{y}(k) \in \mathbb{R}^2$ are the system state, input, and output vectors, respectively. The matrix coefficients are described in terms of system parameters:

$$\boldsymbol{A}_d = \begin{bmatrix} 1 - T_s\frac{R_s}{L_d} & 0 \\ 0 & 1 - T_s\frac{R_s}{L_q} \end{bmatrix},$$

$$\boldsymbol{B}_d = \boldsymbol{B}_\varsigma = \begin{bmatrix} T_s\frac{1}{L_d} & 0 \\ 0 & T_s\frac{1}{L_q} \end{bmatrix}, \quad \boldsymbol{C}_d = \begin{bmatrix} 1 & 0 \\ 0 & 1 \end{bmatrix}.$$

The linear plant model (10) should be augmented with the disturbance model $\boldsymbol{\varsigma}(k)$ to capture the mismatch between (7) and (10) in the steady state. Under certain conditions, the MPC controller in combination with the observer provides zero offset in the steady state. Further details about the conditions and proofs for offset-free MPC can be found in [18]. Our MPC scheme has the following form:

$$\begin{cases} \boldsymbol{x}(k+1) = \boldsymbol{A}_d\boldsymbol{x}(k) + \boldsymbol{B}_d\boldsymbol{u}(k) + \boldsymbol{B}_\varsigma\boldsymbol{\varsigma}(k) \\ \boldsymbol{\varsigma}(k+1) = \boldsymbol{\varsigma}(k) \\ \boldsymbol{y}(k) = \boldsymbol{C}_d\boldsymbol{x}(k) \end{cases} \tag{11}$$

In our MPC problem setup, the plant model is augmented by as many states as there are tracked variables, and the number of disturbances is equal to the number of measurements, which guarantee offset-free control. Theoretical analysis of the offset-free properties of such an augmentation within MPC was performed [20]. To yield the exact open-loop state evolution in (11), the state and disturbance terms are required over the prediction horizon. To this end, we propose an adaptive Kalman observer (AKO), based on augmented model (11), to estimate the states and corresponding disturbances simultaneously at each sampling instant, which is discussed in Subsection IV-A.

IV. PROPOSED EMPC FRAMEWORK

A. DISTURBANCE OBSERVER DESIGN

The observer is used to estimate the states and disturbances from the measured stator currents, which are designed through a Kalman filter. For the LTI system (11), where the number of measurable outputs is equal to the number of disturbances, the existence of stable states and disturbance observations can be proven [18]. Without any loss of generality, the state and disturbance observer is designed based on the augmented model (11) as follows:

$$\begin{cases} \begin{bmatrix} \boldsymbol{x}(k+1) \\ \boldsymbol{\varsigma}(k+1) \end{bmatrix} = \begin{bmatrix} \boldsymbol{A}_d & \boldsymbol{B}_\varsigma \\ 0 & \boldsymbol{I} \end{bmatrix} \begin{bmatrix} \boldsymbol{x}(k) \\ \boldsymbol{\varsigma}(k) \end{bmatrix} + \begin{bmatrix} \boldsymbol{B}_d \\ 0 \end{bmatrix} \boldsymbol{u}(k) + \boldsymbol{w}(k) \\ \boldsymbol{y}(k) = [\boldsymbol{C}_\mathrm{d} \quad 0] \begin{bmatrix} \boldsymbol{x}(k) \\ \boldsymbol{\varsigma}(k) \end{bmatrix} + \boldsymbol{v}(k) \end{cases} \tag{12}$$

where the vectors $\boldsymbol{w}(k) \in \mathbb{R}^4$ and $\boldsymbol{v}(k) \in \mathbb{R}^2$ are zero-mean white-nose disturbance for the augmented system and

measurement, respectively. $\boldsymbol{w}(k)$ and $\boldsymbol{v}(k)$ are not cross correlated and their covariances satisfy the following:

$$\begin{cases} \boldsymbol{Q}_w = cov(\boldsymbol{w}) = E[\boldsymbol{w}\boldsymbol{w}^T] \\ \boldsymbol{R}_v = cov(\boldsymbol{v}) = E[\boldsymbol{v}\boldsymbol{v}^T] \end{cases} \tag{13}$$

where $\boldsymbol{Q}_w \in \mathbb{R}^{4\times4}$ and $\boldsymbol{R}_v \in \mathbb{R}^{2\times2}$ are diagonal matrices. The Kalman observer (KO) consists of the set of simple recursive calculations shown below:

$$\begin{cases} \begin{bmatrix} \hat{\boldsymbol{x}}(k+1) \\ \hat{\boldsymbol{\varsigma}}(k+1) \end{bmatrix} = \begin{bmatrix} \hat{\boldsymbol{x}}(k) \\ \hat{\boldsymbol{\varsigma}}(k) \end{bmatrix} + \boldsymbol{L}(k)\boldsymbol{Err}(k) \\ \hat{\boldsymbol{P}}(k+1) = (\boldsymbol{I} - \boldsymbol{L}(k)\overline{\boldsymbol{C}})\hat{\boldsymbol{P}}(k) \end{cases} \tag{14}$$

where $\hat{\boldsymbol{x}}(k+1)$, $\hat{\boldsymbol{\varsigma}}(k+1)$, and $\hat{\boldsymbol{P}}(k+1) \in \mathbb{R}^{4\times4}$ are the state estimate, disturbance estimate, and error covariance after a measurement update, respectively. Here, $\boldsymbol{L}(k) \in \mathbb{R}^{4\times2}$ are the predictor gain matrices for the state and the disturbance, and $\boldsymbol{Err}(k) \in \mathbb{R}^{2\times1}$ is known as the innovation sequence, which contains the error between the system model predictive output and the plant measurement output. These values are updated as follows:

$$\begin{cases} \begin{bmatrix} \hat{\boldsymbol{x}}(k) \\ \hat{\boldsymbol{\varsigma}}(k) \end{bmatrix} = \begin{bmatrix} \boldsymbol{A}_d & \boldsymbol{B}_\varsigma \\ \boldsymbol{0} & \boldsymbol{I} \end{bmatrix} \begin{bmatrix} \hat{\boldsymbol{x}}(k-1) \\ \hat{\boldsymbol{\varsigma}}(k-1) \end{bmatrix} + \begin{bmatrix} \boldsymbol{B}_d \\ \boldsymbol{0} \end{bmatrix} \boldsymbol{u}(k) \\ \hat{\boldsymbol{P}}(k) = \overline{\boldsymbol{A}}\hat{\boldsymbol{P}}(k-1)\overline{\boldsymbol{A}}^T + \boldsymbol{Q}_w(k) \\ \boldsymbol{L}(k) = \hat{\boldsymbol{P}}(k)\overline{\boldsymbol{C}}^T(\overline{\boldsymbol{C}}\hat{\boldsymbol{P}}(k)\overline{\boldsymbol{C}}^T + \boldsymbol{R}_v(k))^{-1} \\ \boldsymbol{Err}(k) = \boldsymbol{y}_m(k) - \boldsymbol{C}_d\hat{\boldsymbol{x}}(k-1) \end{cases} \tag{15}$$

where $\overline{\boldsymbol{A}} = \begin{bmatrix} \boldsymbol{A}_d & \boldsymbol{B}_\varsigma \\ 0 & \boldsymbol{I} \end{bmatrix}$, $\overline{\boldsymbol{C}} = [\boldsymbol{C}_\mathrm{d}\ \boldsymbol{0}]$;

$\boldsymbol{y}_m(k) \in \mathbb{R}^{2\times1}$ is the measurable output vector; $\hat{\boldsymbol{x}}(k-1)$, $\hat{\boldsymbol{\varsigma}}(k-1)$, and $\hat{\boldsymbol{P}}(k-1)$ are the state estimate, disturbance estimate, and error covariance prior to the measurement update, respectively; and $\boldsymbol{I}$ denotes the unit matrix. A larger $\boldsymbol{Q}_w$ means the prediction generated by the system model is less credible and that the observer attains a fast transient response. However, this will result in ripples in steady state [30]. Similarly, a larger $\boldsymbol{R}_v$ means the measurement results are relatively less credible. For traditional KO, the covariance matrix of the system noise $\boldsymbol{Q}_w$ and covariance matrix of the measurement noise $\boldsymbol{R}_v$ are both treated as constant matrices. For a stable system, $\boldsymbol{R}_v$ is constant because the measurement noise can be determined by trials. However, it is important to consider the parameter uncertainty of the IPMSM motor caused by the current, temperature, and magnetic saturation. Specifically, a large step in i_d and i_q will make L_d and L_q change accordingly, causing $\boldsymbol{\varsigma}(k)$ to vary dramatically. In this situation, because the system model is imprecise, we should adopt a larger $\boldsymbol{Q}_w$ in the transient process to ensure faster convergence. To ensure convergence and reject ripples, a small $\boldsymbol{Q}_w$ should be chosen in the steady state of the KO, which can be identified by $\boldsymbol{Err}(k)$. To overcome the shortcomings of KO, a flexible adaptive mechanism is proposed, based on the traditional KO, to formulate the AKO. The adaptive mechanism is designed as follows:

$$\begin{cases} diag(\boldsymbol{Err}(k)\boldsymbol{Err}(k)^T) \geq [err_{threhold1}, err_{threhold2}]^T, \\ \boldsymbol{Q}_w(k) = (1+\sigma)^*\boldsymbol{Q}_w(k-1) \\ diag(\boldsymbol{Err}(k)\boldsymbol{Err}(k)^T) < [err_{threhold1}, err_{threhold2}]^T, \\ \boldsymbol{Q}_w(k) = (1-\sigma)^*\boldsymbol{Q}_w(k-1) \end{cases} \tag{16}$$

where σ is a scalar tuning parameter for the closed-loop performance. A larger σ will enhance the effectiveness of the tracking but it will also increase sensitivity to system noise. Therefore, by simple manipulation of this single tuning parameter, we can elicit a tradeoff between effectiveness and low sensitivity to noise. In addition, $\boldsymbol{Q}_w(k)$ will be limited by $\boldsymbol{Q}_w(0)$. When starting up, the estimated states and disturbances are initialized by $\hat{\boldsymbol{x}}(0) = [0\ 0]^T$ and $\hat{\boldsymbol{\varsigma}}(0) = [0\ 0]^T$. The AKO algorithm is summarized in Table 1.

TABLE 1. The AKO algorithm.

AKO Algorithm
1. Set the original state $\hat{\boldsymbol{x}}(0)$, $\hat{\boldsymbol{\varsigma}}(0)$, $\boldsymbol{P}(0)$, and $\boldsymbol{Q}_w(0)$ $\boldsymbol{R}_v$;
2.Calculate rotor position, $i_\mathrm{d}(k)$, and $i_q(k)$ using the measured phase current;
3. Obtain the control inputs: $u_\mathrm{d}(k)$ and $u_q(k)$;
4. Calculate $\hat{\boldsymbol{x}}(k)$, $\hat{\boldsymbol{\varsigma}}(k)$, $\hat{\boldsymbol{P}}(k)$, $\boldsymbol{L}(k)$, and $\boldsymbol{Err}(k)$ in (15);
5. if $diag(\boldsymbol{Err}(k)\boldsymbol{Err}(k)^T) \geq [err_{threhold1}, err_{threhold2}]^T$ then
$\boldsymbol{Q}_w(k) = (1+\sigma)^*\boldsymbol{Q}_w(k-1)$;
6. else
$\boldsymbol{Q}_w(k) = (1-\sigma)^*\boldsymbol{Q}_w(k-1)$;
7. if $\boldsymbol{Q}_w(k) \leq \boldsymbol{Q}_w(0)$ then
$\boldsymbol{Q}_w(k) = \boldsymbol{Q}_w(0)$;
8. end if
9. end if
10. $k = k+1$;
11. Calculate $\hat{\boldsymbol{x}}(k+1)$, $\hat{\boldsymbol{\varsigma}}(k+1)$, and $\hat{\boldsymbol{P}}(k+1)$ in (14);
12. Output $\hat{\boldsymbol{x}}(k+1)$ and $\hat{\boldsymbol{\varsigma}}(k+1)$.

B. CONSTRAINT REFORMULATION

The two most important physical constraints of an IPMSM drive system are the current and voltage. The limit of the stator current magnitude, $I_{s\_\max}$, must satisfy the maximum allowable current of the inverter and motor, which is dependent on thermal capability. The stator voltage constraint is related to the maximum available output voltage magnitude of the voltage source inverter. The maximum magnitude of the phase voltage is given as $U_{s\_\max} = V_\mathrm{dc}/\sqrt{3}$, based on space vector modulation without consideration of the overmodulation technique. Here, V_dc is the DC link voltage. We obtain the corresponding constraints represented in the dq-frame circularly as

$$\sqrt{i_d^2 + i_q^2} \leq I_{s\_\max} \tag{17}$$

$$\sqrt{u_d^2 + u_q^2} \leq U_{s\_\max} \tag{18}$$

Unfortunately, (17) and (18) cannot be modeled directly as a function of constraints because they are nonlinear;

however, a polytopic approximation of constraints can be employed [23]. The two circulars in (17) and (18) can be approximated by polygons inscribed in the circles. The larger the order N of the inscribed polygon, the more accurate the approximation, but the export LUT of the PWA control law will increase dramatically, resulting in high requirement for microprocessor memory. Here, by choosing $N = 8$, the quadratic inequalities can be converted into a series of linear inequalities given as follows:

$$\begin{bmatrix} 0 & -\frac{1}{\sqrt{2}} & -1 & -\frac{1}{\sqrt{2}} & 0 & \frac{1}{\sqrt{2}} & 1 & \frac{1}{\sqrt{2}} \\ 1 & \frac{1}{\sqrt{2}} & 0 & -\frac{1}{\sqrt{2}} & -1 & -\frac{1}{\sqrt{2}} & 0 & \frac{1}{\sqrt{2}} \end{bmatrix}^T \times \begin{bmatrix} u_d(k) \\ u_q(k) \end{bmatrix} \leq \boldsymbol{T} \times U_{s\_max} \tag{19}$$

$$\begin{bmatrix} 0 & -\frac{1}{\sqrt{2}} & -1 & -\frac{1}{\sqrt{2}} & 0 & \frac{1}{\sqrt{2}} & 1 & \frac{1}{\sqrt{2}} \\ 1 & \frac{1}{\sqrt{2}} & 0 & -\frac{1}{\sqrt{2}} & -1 & -\frac{1}{\sqrt{2}} & 0 & \frac{1}{\sqrt{2}} \end{bmatrix}^T \times \begin{bmatrix} i_d(k) \\ i_q(k) \end{bmatrix} \leq \boldsymbol{T} \times I_{s\_max} \tag{20}$$

where $\boldsymbol{T} = \cos(\frac{\pi}{8}) \times [\,1\ 1\ 1\ 1\ 1\ 1\ 1\ 1\,]^T$.

C. CONTROLLER SYNTHESIS

1) STATE AUGMENTATION FOR TRACKING

The plant model is augmented with a disturbance model $\boldsymbol{\varsigma}(k)$ as shown in (11); the estimated $\hat{\varsigma}_d(k)$ and $\hat{\varsigma}_q(k)$ of $\boldsymbol{\varsigma}(k)$ thus need to be introduced to the state vector. The control objective is to make the measured outputs $\boldsymbol{y}_{\mathrm{m}}(k)$ track the constant reference $\boldsymbol{x}_{ref}(k) = \begin{bmatrix} i_d^{ref}(k) & i_q^{ref}(k) \end{bmatrix}^T$. Therefore, it is also necessary to augment the reference in the state vector to be able to penalize the error in the cost function. Even if states i_d and i_d are available from measurement at each sampling instant, the noise should be filtered out. Therefore, we prefer to use the state estimate $\hat{\boldsymbol{x}}(k)$ as the current state. The MPC problem is solved explicitly with respect to the EMPC concept, resulting in a PWA control law of the new augmented state vector $\boldsymbol{x}_{Tar}(k) = \begin{bmatrix} \hat{i}_d & \hat{i}_q & \hat{\varsigma}_d & \hat{\varsigma}_q & i_d^{ref} & i_q^{ref} \end{bmatrix}^T$. According to the choice of $\boldsymbol{x}_{Tar}$ as the state vector of the system, the corresponding state update equation and output equations have the following form:

$$\begin{cases} \boldsymbol{x}_{Tar}(k+1) = \begin{bmatrix} \boldsymbol{A}_d & \boldsymbol{B}_\zeta & \boldsymbol{O}_{2\times2} \\ \boldsymbol{O}_{2\times2} & \boldsymbol{I}_{2\times2} & \boldsymbol{O}_{2\times2} \\ \boldsymbol{O}_{2\times2} & \boldsymbol{O}_{2\times2} & \boldsymbol{I}_{2\times2} \end{bmatrix} \boldsymbol{x}_{Tar}(k) + \begin{bmatrix} \boldsymbol{B}_d \\ \boldsymbol{O}_{2\times2} \\ \boldsymbol{O}_{2\times2} \end{bmatrix} \boldsymbol{u}(k) \\ \boldsymbol{y}_{Tar}(k) = \begin{bmatrix} \boldsymbol{C}_d & \boldsymbol{O}_{2\times2} & \boldsymbol{O}_{2\times2} \end{bmatrix} \boldsymbol{x}_{Tar}(k) \end{cases} \tag{21}$$

where $\boldsymbol{O}$ and $\boldsymbol{I}$ represent the identity and zero matrices, respectively, whereas $\boldsymbol{A}_d$, $\boldsymbol{B}_\zeta$, and $\boldsymbol{B}_d$ are the matrices that appear in (10). The starting points of the predictive states and disturbances in the MPC problem are initialized by the AKO estimates.

2) TARGET CALCULATION FOR OFFSET-FREE MPC

From (14) and (15), we note that the disturbance estimate $\hat{\boldsymbol{\zeta}}(k)$ converges only if $\boldsymbol{y}_m(k) - C_d\hat{\boldsymbol{x}}(k) = 0$; then, the steady state of the observer (14) and (15) satisfies [18]:

$$\begin{bmatrix} \boldsymbol{A}_d - \boldsymbol{I} & \boldsymbol{B}_d \\ \boldsymbol{C}_d & \boldsymbol{0} \end{bmatrix} \begin{bmatrix} \hat{\boldsymbol{x}}_\infty \\ \boldsymbol{u}_\infty \end{bmatrix} = \begin{bmatrix} -\boldsymbol{B}_\varsigma \hat{\boldsymbol{\zeta}}_\infty \\ \boldsymbol{y}_{m,\infty} \end{bmatrix} \tag{22}$$

where we have denoted the steady state value with subscript ∞. $\boldsymbol{y}_{m,\infty}$ and $\boldsymbol{u}_\infty$ are the steady-state measured output and control input of system (7), respectively; and $\hat{\boldsymbol{x}}_\infty$ and $\hat{\boldsymbol{\zeta}}_\infty$ are the state and disturbance estimates from the observer at the steady-state, respectively. By replacing $\boldsymbol{x}_\infty$ with $\boldsymbol{x}_{ref}(k)$, $\boldsymbol{y}_{m,\infty}$ with $C_d\boldsymbol{x}_{ref}(k)$, and $\hat{\boldsymbol{\zeta}}_\infty$ with $\hat{\boldsymbol{\zeta}}(k)$, we can obtain the following:

$$\begin{bmatrix} \boldsymbol{A}_d - \boldsymbol{I} & \boldsymbol{B}_d \\ \boldsymbol{C}_d & \boldsymbol{0} \end{bmatrix} \begin{bmatrix} \boldsymbol{x}_{ref}(k) \\ \boldsymbol{u}_{Tar}(k) \end{bmatrix} = \begin{bmatrix} -\boldsymbol{B}_\varsigma \hat{\boldsymbol{\zeta}}(k) \\ \boldsymbol{C}_d\boldsymbol{x}_{ref}(k) \end{bmatrix} \tag{23}$$

where $\boldsymbol{u}_{Tar}(k)$ is the target control input and $\hat{\boldsymbol{\zeta}}(k)$ accounts for all effects responsible for deviations from the reference. By solving (23) and incorporating the obtained $\boldsymbol{u}_{Tar}(k)$ into the cost function, the estimated state $\hat{\boldsymbol{x}}(k)$ and the control input $\boldsymbol{u}(k)$ can both be penalized for deviations from the reference $\boldsymbol{x}_{ref}(k)$and the target control input $\boldsymbol{u}_{Tar}(k)$. Therefore, the cost function (2) is rewritten in the following form:

$$\begin{aligned} &J(\boldsymbol{U}, \boldsymbol{x}(k)) \\ &= \sum_{i=1}^{N_p} [(\hat{\boldsymbol{x}}(k+i) - \boldsymbol{x}_{ref}(k))^T \overline{\boldsymbol{Q}} (\hat{\boldsymbol{x}}(k+i)^T - \boldsymbol{x}_{ref}(k)) \\ &\quad + (\boldsymbol{u}(k+i-1) - \boldsymbol{u}_{Tar}(k))^T \overline{\boldsymbol{R}} (\boldsymbol{u}(k+i-1) - \boldsymbol{u}_{Tar}(k))] \end{aligned} \tag{24}$$

where $\overline{\boldsymbol{Q}} \in \mathbb{R}^{2\times2}$ and $\overline{\boldsymbol{R}} \in \mathbb{R}^{2\times2}$ are the positive definite diagonal penalties. The observer estimates the state and disturbance by feeding the error between the measured and estimated output at each time step to make $\boldsymbol{C}_{\mathrm{d}}\hat{\boldsymbol{x}}(k) \rightarrow \boldsymbol{y}_m(k)$. The MPC controller calculates the optimal control input to make $\boldsymbol{C}_d\hat{\boldsymbol{x}}(k) \rightarrow \boldsymbol{x}_{ref}(k)$. The combination of the observer/controller can make $\boldsymbol{y}_m(k) \rightarrow \boldsymbol{x}_{ref}(k)$. In summary, the state update can be obtained from (21), the target calculator derived from (23), the constraints follow (19) and (20), and the cost function is given by (24). Thus, all the elements for EMPC formulation are ready. Then, the closed-loop system was obtained by controlling (7) with this EMPC controller and the observer (14) and (15). When the value of the cost function is zero, it means that the measured outputs reach their reference values and that the observer enters the steady state. Furthermore, the effect of the disturbance is canceled by MPC optimization, and the controlled variables are tracked at their reference despite model mismatches. Further details regarding proof of the convergence of such MPC closed-loop systems are discussed in [18]. A general block diagram of

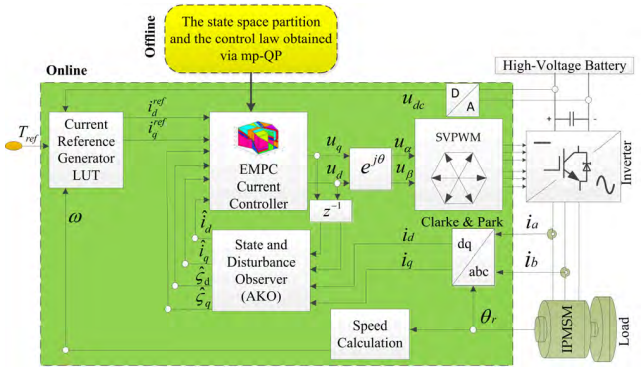

FIGURE 1. Structure block diagram of the proposed explicit model predictive current control system.

the proposed control scheme can be divided into two stages: offline and online, as shown in Fig. 1.

In the offline stage, the EMPC controller can be formulated and solved via MPT in conjunction with the appropriate solver. For fine-tuning the cost function and the constraints, the YALMIP toolbox of MATLAB [31] are invoked. The optimal EMPC laws are computed explicitly offline and they can be exported as completely MPT-independent C-program code for online implementation or as an m-file for simulation using MATLAB/Simulink. In the online stage, the current reference LUT maps the current reference in the dq-frame according to the required torque (represented by T_{ref}). The current reference generation is based on the results of another study [32], which consider the impact of DC-link voltage changes for a wide speed range operation, i.e., the flux-weakening region. AKO estimates both the states and the disturbances, enhancing robustness against uncertainties and measurement noise. The actual active region is searched according to the updating parameter vector $\boldsymbol{x}_{Tar}$, following which the corresponding optimal control law is obtained. The space vector modulation technique is used to excite the motor via an inverter. The online integration algorithm is summarized in Table 2.

TABLE 2. Online integration algorithm.

Online Integration Algorithm for each sample instant k
1. Measure $\mathbf{y}_{\mathrm{m}}(k)$ and the rotor position;
2. Obtain $\mathbf{x}_{ref}(k)$ according to the reference generator (LUT);
3. Execute the AKO algorithm;
4. Read the results from AKO to obtain $\hat{\boldsymbol{x}}(k+1)$ and $\hat{\varsigma}(k+1)$;
5. Construct the current state vector $\boldsymbol{x}_{Tar}(k)$ for EMPC;
6. Locate the active region number i according to $\boldsymbol{x}_{Tar}(k)$;
7. Consult the LUT to determine the optimal control input $\boldsymbol{u}^*(k)$ via the returned i;
8. Implement field-oriented control with $\boldsymbol{u}^*(k)$ as the control input voltage.

V. SIMULATION AND EXPERIMENT

A. SIMULATION RESULTS

We simulated working with the EMPC controller using MATLAB/Simulink. The motor parameters are given in Table 3.

TABLE 3. Parameters of the machine.

Parameter	Value	Parameter	Value
DC bus voltage	330 V	Permanent magnet flux	0.0682 Wb
Pole pairs	4	d-axis inductance	0.000067 H
Nominal torque	100 N·m	q-axis inductance	0.000237 H
Nominal speed	4000 rpm	Total moment of inertia	0.04 kg·m^2
Nominal power	40 kW	Maximum phase current	410 A

A time step $T_s = 100\mu s$ was chosen in this study. According to Table 3, we set the voltage constraint $U_{s\_\max} = 330V/\sqrt{3}$ and the current constraint $I_{s\_\max} = 410A$. The quantities to be weighted are the current error $\hat{\boldsymbol{x}} - \boldsymbol{x}_{ref}$ and voltage error $\boldsymbol{u} - \boldsymbol{u}_{Tar}$ in the cost function. The ratio between the matrices $\overline{\boldsymbol{Q}}$ and $\overline{\boldsymbol{R}}$ measures the tradeoff between rapidity and sensitivity. A large $\overline{\boldsymbol{Q}}$ implies a fast controller. The weighting matrices were set as $\overline{\boldsymbol{Q}} = diag(0.95, 0.85)$, and $\overline{\boldsymbol{R}} = diag(1, 1)$. Ideally, the length N_{p} of the prediction horizon should be chosen long enough to include the most relevant part of the system dynamics. However, that would result in a large number of time steps. The effects of changes in the control input signals u_d and u_q at the time step k will have effect on the currents i_d and i_q at the time step $k+1$. This requires a minimum value of $N_{\mathrm{p}} = 2$ for the prediction horizon. Therefore, we chose $N_{\mathrm{p}} = 3$ in our implementation. The control horizon N_u is the number of steps after which the input signal is considered steady when predicting the future response of the system. The only reason for using the parameter N_u is the simplification of the optimization process. Considering that $N_u \leq N_{\mathrm{p}}$ is theoretical properties in MPC, so in our study, it was set to $N_u = 1$. The initial parameters of AKO were $[err_{threshold1}, err_{threshold2}]^T = [0.8, 0.8]^T$, $\boldsymbol{R}_v = diag(0.5, 0.5)$, $\sigma = 0.8$ and $\boldsymbol{Q}_w = diag(1.2,1.2,1.31,1.35)$. The EMPC controller solved by the MPT toolbox returns explicit parametric solutions resulting in 1287 polyhedral regions and the associated affine control laws stored in an LUT defined on a 6-dimensional state–space partition. The simulation was undertaken out under the scenario shown in Fig. 2. At the initial stage, the rotor speed is 3000 rpm and the reference torque is 0 N · m. Then, the reference torque is changed abruptly to its peak value of 192 N · m at 0.05 s and it remains unchanged for 0.2 s, after which the reference torque drops abruptly to 47 N · m (at 0.25 s). Between the times of 0.3 and 1.3 s, the rotor speed increases from 3000 to 6000 rpm, i.e., higher than the rated speed. After a short time, the reference torque increases from 47 to 101 N · m before decreasing to 67 N · m in the form of a step. The reference torque and the related mapped reference current with the setting time are shown in Table 4, where the reference d- and q-axis currents are denoted as i_d^{ref} and i_q^{ref}, respectively.

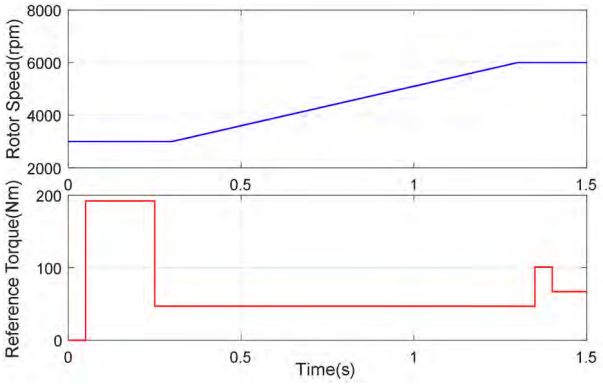

FIGURE 2. Scenario for rotor mechanical velocity and the reference torque input. From top to bottom: rotor speed and reference torque.

TABLE 4. Reference torque and corresponding reference current mapping relationship with setting time at different rotor speeds.

Reference Torque (N·m)	Rotor Speed (rpm)	i_d^{ref} (A)	i_q^{ref} (A)	Setting time (s)
192	3000	−243	330	0.05
47	3000–6000	−66	134	0.25
101	6000	−185	199	1.35
67	6000	−134	153	1.40

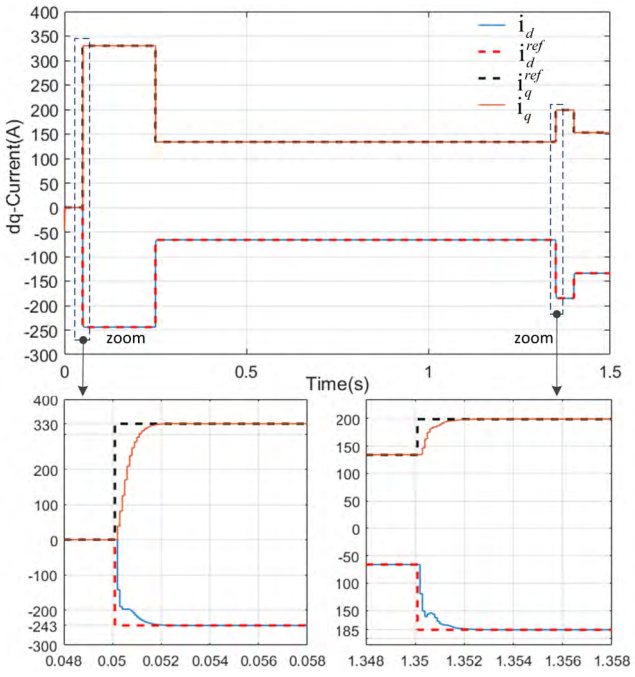

FIGURE 3. dq-axis current responses to a series of reference current pulses with the rotor running at different speeds from 3000 to 6000 rpm.

Figure 3 shows a series of d- and q-axis current step response results. We can see that the measured current can track the reference very well. In the 1.0-s period after the instant at 0.3 s, the rotor speed rises rapidly from 3000 to 6000 rpm. In this case, the rapid change in rotor speed causes a drastic change in the disturbance $\varsigma(k)$. However, from 0.3 to 1.3 s, the measured current could still accurately

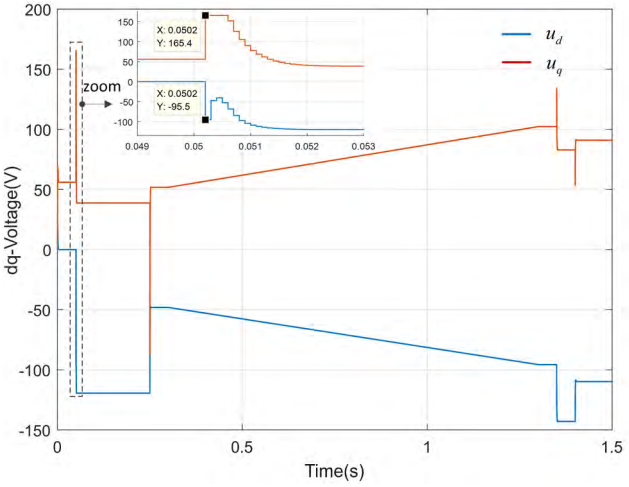

FIGURE 4. dq-axis voltage responses to a series of reference current pulses with the rotor running at different speeds from 3000 to 6000 rpm.

track the reference without fluctuation or steady-state error, indicating the controller has strong robustness against parameter variations. The results at approximately 0.05 and 1.35 s are shown enlarged in the lower panels for further analysis. At 0.05 s, the maximum amplitude of the stator reference current is $I_s = \sqrt{(i_d^{ref})^2 + (i_q^{ref})^2} = 410A$. Thus, the current constraint is triggered, but the EMPC controller ensures that $\sqrt{i_d^2 + i_q^2}$ does not exceed the limit of 410 A. In the lower-right panel of Fig. 3 (at 1.35 s), the step response where the amplitude is increased after the rotor speed is stabilized at 6000 rpm (higher than the nominal speed) exhibits good tracking performance with the IPMSM operating in the flux-weakening regions. The corresponding control input voltage waveform is shown in Fig. 4. The control voltage can respond quickly with very limited fluctuations in each of the d- and q-axis current reference steps. From the zoomed-in inset at 0.05 s, it can be seen that the maximum amplitude of the stator phase voltage at 0.0502 s is $U_s = \sqrt{u_d^2 + u_q^2} = 191V$, which means the voltage constraint $U_{s\_\max}$ is active. However, the voltage and current constraints are strictly satisfied at each sampling interval with the imposed bounds of $U_{s\_\max} = 191V$ and $I_{s\_\max} = 410A$, respectively. The waveforms in Figs. 3 and 4 indicate the controller has excellent capability in handling both the voltage and the current constraints while making full use of the maximum available voltage.

Zero-Offset Control With Parameter Mismatch: The accurate mathematical model of IPMSM is dependent on the electrical parameters. However, these parameters might not match their actual values owing to measurement errors or changes in the different operation points. All these model parameter mismatches and uncertainties will deteriorate the performance of the controller. The next simulation further evaluates the closed-loop current tracking and zero-offset control in the case of a plant model with parameter mismatch. For this simulation, the d- and q-axis inductances are disturbed by $L_{d1} = 1.3{*}L_d$ and $L_{q1} = 0.8{*}L_q$ in the plant model. The values of

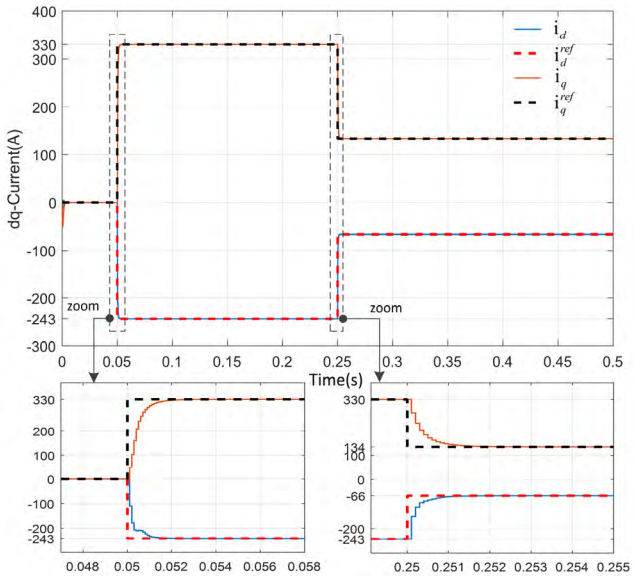

FIGURE 5. dq-axis current tracking performance for plant model with d- and q-axis inductance parameter mismatch.

L_d and L_q remain unchanged in the AKO model (14) and (15) and the predictive model (21), i.e., their values are consistent with those in Table 3. The simulation runs as follows. When the rotor speed is stable at 3000 rpm, the current references step away from 0 to the peak value ($i_d = -243$A, $i_q = 330$A) at 0.05 s. Then, the current references step back from the peak value to $i_d = -66$A, $i_q = 134$A at 0.25 s. The d- and q-axis current response waveforms are shown Fig. 5. It can be seen that the proposed EMPC controller remains able to achieve zero-offset control in the case of parameter mismatch.

We also investigated the observed state from the AKO in the cases with parameter mismatch and with normal parameters. Figure 6 illustrates the observed d- and q-axis current waveforms from the AKO, with zoomed-in areas of time at approximately 0.05 s. These results show that the observed state values both can converge to the reference values in the presence of parameter mismatch. By comparing the waveforms of Figs. 6(a) and Figs. 6(b), it can be seen that parameter mismatch causes the convergence of the observation result to be slower than the result with the normal parameter. However, these have no effect on the performance of the system in the steady state.

The curves shown in Fig. 7 depict the observed disturbance term waveforms from the AKO. Here, $\hat{\varsigma}_{d1}$ and $\hat{\varsigma}_{q1}$ denote the results with parameter mismatch and $\hat{\varsigma}_d$ and $\hat{\varsigma}_q$ are the results with normal parameters. Figure 8 shows the profiles of the corresponding control input dq-voltage, where u_{d1} and u_{q1} represent the control input voltages in the case of parameter mismatch, and u_d and u_q denote the control input voltages with normal parameters. As shown in Figs. 7 and 8, the difference between the amplitudes of $\hat{\varsigma}_d$ and $\hat{\varsigma}_{d1}$ is the same as that between the amplitudes of u_d and u_{d1}, the same is true in the case of the q-axis at steady state. This reveals that the estimated disturbance $\hat{\boldsymbol{\varsigma}}$ captures the error between

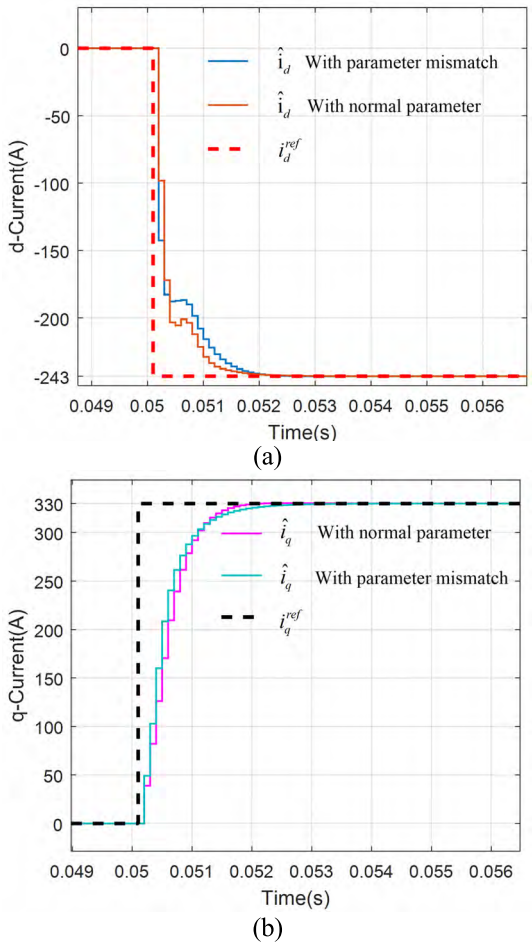

FIGURE 6. Comparisons of the observed dq-current step responses between the plant model with normal parameters and with parameter mismatch: (a) d-axis current waveforms and (b) q-axis current waveforms.

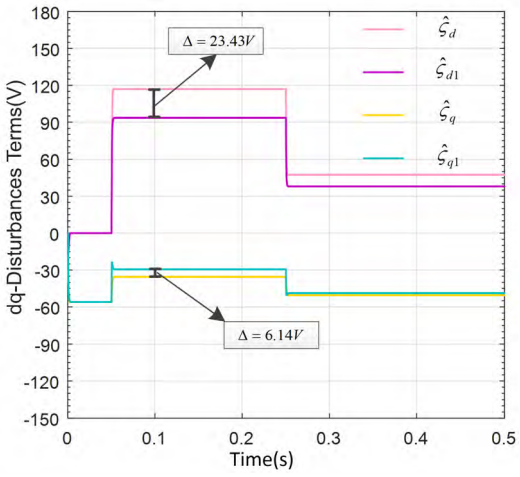

FIGURE 7. Comparison between observed disturbance terms of the plant model with parameter mismatch and with normal parameters.

the prediction and the plant model in the steady state, and that the obtained optimal control input voltage from the EMPC is compensated accordingly in the closed-loop process when the voltage constraint is not activated at the steady state.

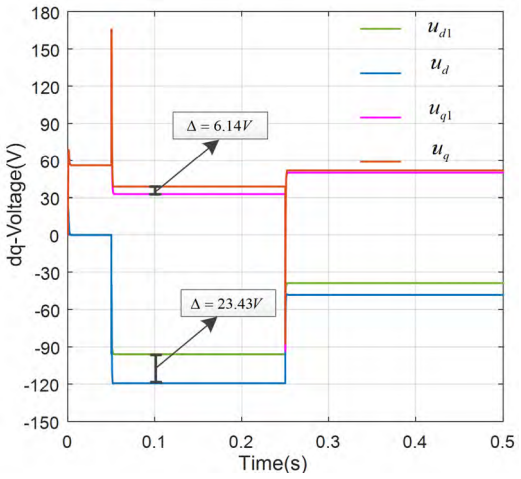

FIGURE 8. Comparison between dq-voltages of the plant model with parameter mismatch and with normal parameters.

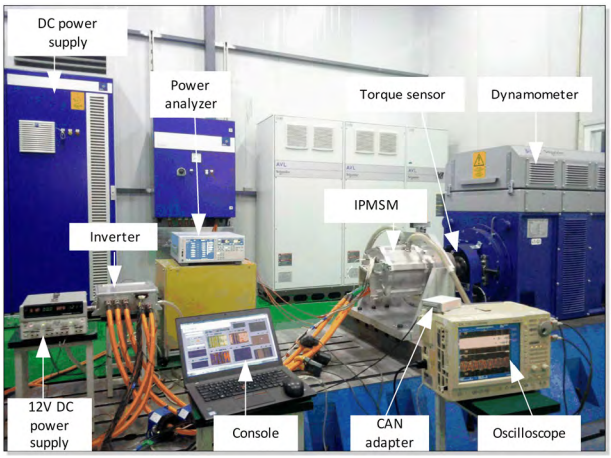

FIGURE 9. Picture of the experimental setup.

B. EXPERIMENTAL RESULTS

In addition to the simulations, the experiments were conducted on a laboratory test bench. The experimental setup is shown in Fig. 9. The AVL dynamometer runs in speed mode as the load and it drags the experimental IPMSM to the target speed. The console on the laptop sends the reference torque via CAN communication to control the voltage-source inverter to drive the IPMSM. The control algorithm is implemented on an Infineon high-performance microcontroller (Tricore TC1782) integrated in the inverter. For the experiment, we set $\overline{\boldsymbol{Q}} = diag(1.15, 1.05)$, for faster dynamic response and we set $\overline{\boldsymbol{R}} = diag(0.9, 0.9)$, to reduce the sensitivity. All other parameters of EMPC, AKO, and IPMSM were identical to those in the simulation. In the following, some experimental results are presented. In the first test, the IPMSM is driven under the same test scenario as in the simulation reported in Fig. 2 and Table 4 to validate the EMPC controller performance in a real-time implementation. In the second test, the control performance of the proposed control scheme is compared with the classic cross-PI feed-forward algorithm to investigate its advantages.

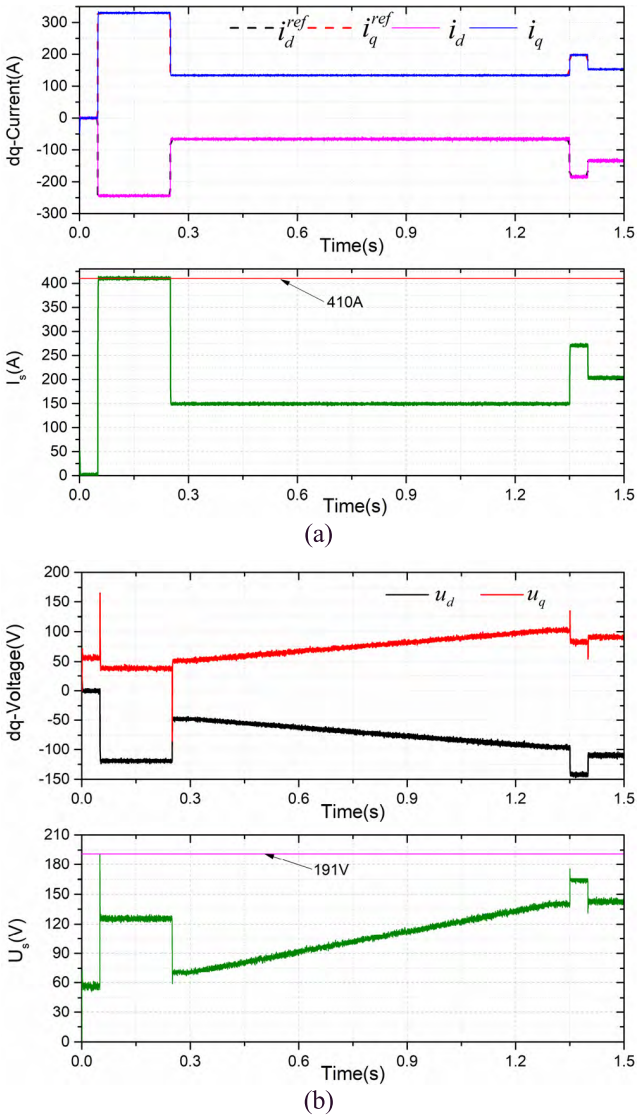

FIGURE 10. Experimental results with proposed EMPC control scheme: (a) dq-currents (upper) and amplitude of the phase current (lower) and (b) dq-voltages (upper) and amplitude of the phase voltage (lower).

For the first test, owing to the state and disturbance observer, the proposed EMPC scheme shows good robustness against parameter mismatches and measurement noise. Consequently, the current reference and dq-current obtained by calculating the measured phase current cannot be distinguished at the steady state, even during the fast speed acceleration stage as shown in upper panel of Fig. 10(a). As shown in the upper panel of Fig. 10(b), the waveforms of the d- and q-axis voltages are consistent with the trend of the simulation profiles presented in Fig. 4. The amplitudes of the stator phase current and voltage, i.e., $I_s = \sqrt{i_d^2 + i_q^2}$ and $U_s = \sqrt{u_d^2 + u_q^2}$, are illustrated with the bounds of the constraints in the lower panels of Fig. 10(a) and 10(b). The slight deviation beyond the imposed bounds is due to noise. Although the fluctuations of the d- and q-axis voltages are slightly higher than the ones in the simulation, the stator

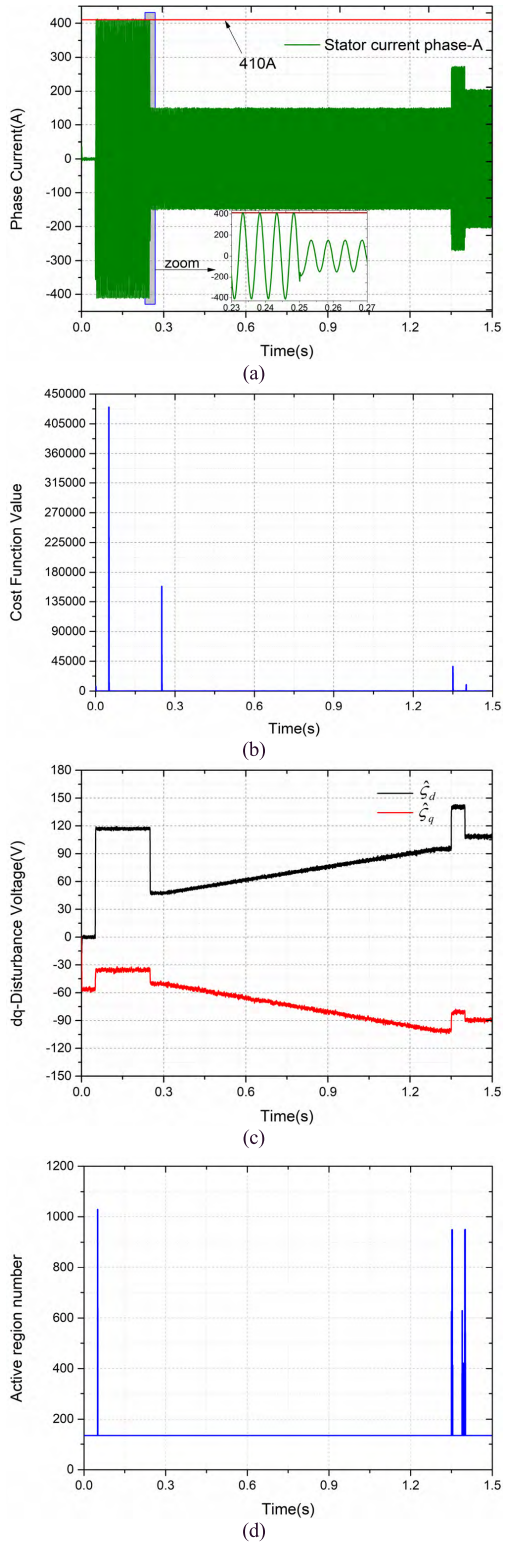

FIGURE 11. Experimental results: (a) one-phase current, (b) cost function value, (c) observed disturbance terms, and (d) active region.

voltage is well constrained throughout the process, especially in the transient procedure.

During the first current step, both the voltage and current constraints were active, but constraint violations were anticipated and prevented. These results indicate that proposed EMPC scheme has the impressive capability of offering multi-input multi-output control as well as handling multiple constraints. Figure 11(a) shows the current curves in one phase. The maximum amplitude of the phase current is well limited to 410 A. The output phase current fluctuates very little at the steady state, i.e., the dynamic process responds quickly without overshooting. It can be seen in Fig. 11(b) that the actual cost function value of the closed-loop system increases dramatically to a reasonably large value in each step process, but then reduces to zero when the dq-currents track to their references at the steady state. It is evident that the optimization problem in MPC is to minimize a finite-horizon cost of the state and control trajectory while satisfying the constraints. Figure 11(c) depicts the waveforms of the estimated disturbance terms, which quickly converge to constants while the system enters steady state. In particular, $\hat{\varsigma}_d$ changes linearly with the uniformly increasing rotor speed because the reference currents do not change during the period of rapid acceleration from 0.3 to 1.3 s. In Fig. 11(d), the indices of the active region at different time instants are shown, which imply that a series of control methods are used in the dynamic response process.

For the second test, a control scheme using the cross-PI feedforward algorithm is compared with the proposed MPC control scheme. The structure of the cross-PI feedforward control scheme is depicted in Fig. 12.

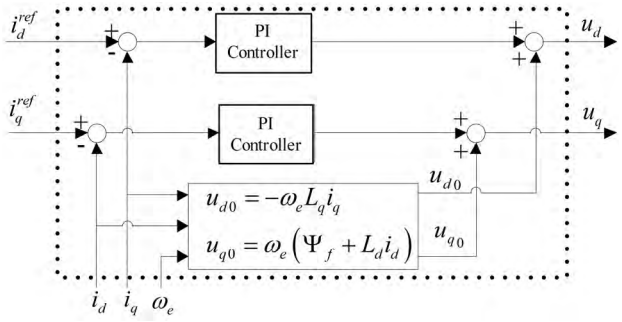

FIGURE 12. Block diagram of cross-PI feedforward controller.

The IPMSM is dragged to 3000 rpm by the dynamometer and controlled by the proposed EMPC scheme and cross-PI feedforward scheme in the form of a current closed loop. The current reference steps from $i_{\mathrm{d}}^{ref} = 0\mathrm{A}$, $i_q^{ref} = 0\mathrm{A}$ to $i_d^{ref} = -249\mathrm{A}$, $i_q^{ref} = 185\mathrm{A}$ at 0.01 s, and then to $i_d^{ref} = -154\mathrm{A}$, $i_q^{ref} = 185\mathrm{A}$ at 0.03 s. Figure 13 shows the experimental waveforms of the currents and control voltages in the dq-frame under these two algorithms. The current control performance of the proposed MPC scheme is compared with the cross-PI feedforward scheme featured in Fig. 13(a). Note that the control gains of the PI controller are designed based on the pole placement technique. It can be seen that the current response of the proposed MPC scheme is much faster and accompanied with better damping characteristics than in the cross-PI feedforward control scheme; this is because there is no integral path in the EMPC, which can avoid overshoot and

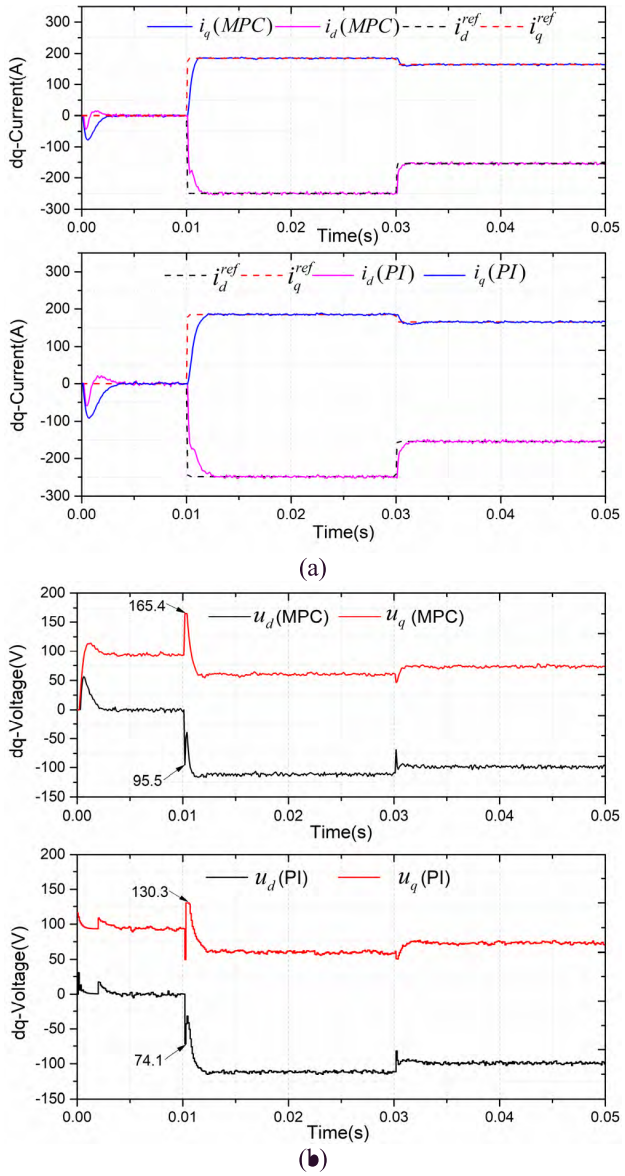

FIGURE 13. Comparison of experimental results under two algorithms: (a) dq-currents with proposed MPC algorithms (upper) and cross-PI feedforward algorithms (lower) and (b) dq-voltages with proposed MPC algorithms (upper) and cross-PI feedforward algorithms (lower).

windup issues. Figure 13(b) shows the corresponding control voltages u_d and u_q applied to the stator of the IPMSM after being modulated by space vector pulse width modulation. The upper panel shows that the proposed MPC algorithms can make the best use of the DC-link voltage to achieve a faster current response while satisfying voltage constraints; therefore, the amplitude change of d- and q-voltages given by the MPC controller is larger than the ones of the PI controller in transients.

The lower panel of Fig. 13(a) shows that the cross-PI feedforward algorithms can also obtain a reasonably rapid and monotonic response. However, to prevent the controller from losing control due to integral saturation, it does not allow using the full available inverter voltage like the EMPC in transients, as shown in the lower panel of Fig. 13(b). In PI controllers, the system constraints are considered based on the saturation of the corresponding values and anti-windup in case of actuating value saturation to suppress output overshooting. The PI algorithms cannot explicitly enforce multiple constraints on the dynamics of the systems, resulting in a current response that is slower than that of MPC.

VI. CONCLUSION

In this paper, we proposed a novel methodology for controller synthesis based on EMPC for current control of an IPMSM. The state–space models of the IPMSM, including the related constraints of the stator current and stator voltage, were linearized under reasonable assumptions. The linearization method of the IPMSM model and the polyhedron approximation method of the quadratic constraints significantly simplify the overall control structure and achieve satisfactory results. Through augmentation of the system via extension with as many additional states as there are tracked variables with respect to offset-free reference tracking, we designed an EMPC controller with an improved disturbance observer combination, which led to a stable closed-loop system for zero steady-state offset, even in the presence of parameter mismatches. The number of state parameter vectors is only six, which considerably reduces the complexity of the EMPC problem. The proposed EMPC algorithm is easy to implement on a real-time platform because it significantly reduces the online computation time compared with the standard MPC method. Simulation and experimental results showed that the proposed EMPC strategy demonstrates high precision in reference tracking and reasonable dynamic performance, as well as high robustness against disturbances resulting from parameter mismatches and sensor noise. Moreover, it was effective in achieving excellent performance in comparison with the state-of-the-art cross-PI feedforward algorithm. Therefore, the proposed control method shows promise for applications such as IPMSM-based automotive electrical traction drives.

REFERENCES

[1] M. Cheng, L. Sun, G. Buja, L. Song, and K. Zhou, "Advanced electrical machines and machine-based systems for electric and hybrid vehicles," *Energies*, vol. 9, no. 8, pp. 9541–9564, Sep. 2015. doi: 10.3390/en8099541.

[2] S. Morimoto, Y. Takeda, T. Hirasa, and K. Taniguchi, "Expansion of operating limits for permanent magnet motor by current vector control considering inverter capacity," *IEEE Trans. Ind. Appl.*, vol. 26, no. 5, pp. 866–871, Sep. 1990.

[3] M. N. Uddin and R. S. Rebeiro, "Performance analysis of an FLC based online adaptation of both hysteresis and PI controllers for IPMSM drive," *IEEE Trans. Ind. Appl.*, vol. 48, no. 1, pp. 12–19, Jan/Feb. 2012. doi: 10.1109/TIA.2011.2175876.

[4] X. Sun, Z. Shi, L. Chen, and Z. Yang, "Internal model control for a bearingless permanent magnet synchronous motor based on inverse system method," *IEEE Trans. Energy Convers.*, vol. 31, no. 4, pp. 1539–1548 Dec. 2016. doi: 10.1109/TEC.2016.2591925.

[5] S. Barkat, A. Tlemçani, and H. Nouri, "Noninteracting adaptive control of PMSM using interval type-2 fuzzy logic systems," *IEEE Trans. Fuzzy Syst.*, vol. 19, no. 5, pp. 925–936, Oct. 2011. doi: 10.1109/TFUZZ.2011.2152815.

[6] X. Zhang, L. Sun, K. Zhao, and L. Sun, "Nonlinear speed control for PMSM system using sliding-mode control and disturbance compensation techniques," *IEEE Trans. Power Electron.*, vol. 28, no. 3, pp. 1358–1365, Mar. 2013.

[7] X. Sun, L. Chen, H. Jiang, Z. Yang, J. Chen, and W. Zhang, "High-performance control for a bearingless permanent-magnet synchronous motor using neural network inverse scheme plus internal model controllers," *IEEE Trans. Ind. Electron.*, vol. 63, no. 6, pp. 3479–3488 Jun. 2016. doi: 10.1109/TIE.2016.2530040.

[8] X. Sun, L. Chen, Z. Yang, and H. Zhu, "Speed-sensorless vector control of a bearingless induction motor with artificial neural network inverse speed observer," *IEEE/ASME Trans. Mechatron.*, vol. 18, no. 4, pp. 1357–1366 Aug. 2013. doi: 10.1109/TMECH.2012.2202123.

[9] S. Mariethoz, A. Domahidi, and M. Morari, "High-bandwidth explicit model predictive control of electrical drives," *IEEE Trans. Ind. Appl.*, vol. 48, no. 6, pp. 1980–1992, Nov./Dec. 2012.

[10] F. Bayat and T. A. Johansen, "Multi-resolution explicit model predictive control: Delta-model formulation and approximation," *IEEE Trans. Autom. Control*, vol. 58, no. 11, pp. 2979–2984, Nov. 2013.

[11] E. Carlos Garcia, D. M. Prett, and M. Morari, "Model predictive control: Theory and practice-A survey," *Automatica*, vol. 25, no. 3, pp. 335–348, May 1989. doi: 10.1016/0005-1098(89)90002-2.

[12] D. Q. Mayne, J. B. Rawlings, C. V. Rao, and P. O. M. Scokaert, "Constrained model predictive control: Stability and optimality," *Automatica*, vol. 36, no. 6, pp. 789–814, 2000.

[13] A. Bemporad, F. Borrelli, and M. Morari, "Model predictive control based on linear programming-The explicit solution," *IEEE Trans. Autom. Contro.*, vol. 47, no. 12, pp. 1974–1985, Jan. 2002. doi: 10.1109/TAC.2002.805688.

[14] A. Bemporad, M. Morari, V. Dua, and E. N. Pistikopoulos, "The explicit linear quadratic regulator for constrained systems," *Automatica*, vol. 38, no. 1, pp. 3–20, Jan. 2002.

[15] S. Bolognani, S. Bolognani, L. Peretti, and M. Zigliotto, "Design and implementation of model predictive control for electrical motor drives," *IEEE Trans. Ind. Electron.*, vol. 56, no. 6, pp. 1925–1936, Jun. 2009.

[16] Z. Mynar, L. Vesely, and P. Vaclavek, "PMSM model predictive control with field-weakening implementation," *IEEE Trans. Ind. Electron.*, vol. 63, no. 8, pp. 5156–5166, Aug. 2016. doi: 10.1109/TIE.2016.2558165.

[17] M. R. Rajaman, J. Rawlings, and S. Qin, "Achieving state estimation equivalence for misassigned disturbances in offset-free model predictive control," *Aiche J.*, vol. 55, no. 2, pp. 396–407, Feb. 2009. doi: 10.1002/aic.11673.

[18] U. Maeder, F. Borrelli, and M. Morari, "Linear offset-free model predictive control," *Automatica*, vol. 45, no. 10, pp. 2214–2222, 2009.

[19] G. Pannocchia and A. Bemporad, "Combined design of disturbance model and observer for offset-free model predictive control," *IEEE Trans. Autom Control.*, vol. 18, no. 52, pp. 1048–1053, Jun. 2007. doi: 10.1109/TAC.2007.899096.

[20] J. R. Pannocchia and T. A. Gabriele, "Disturbance modeling for offset-free linear model predictive control," *Aiche J.*, vol. 49, no. 2, pp. 426–437, Apr. 2004. doi: 10.1002/aic.690490213.

[21] S. Mariéthoz, A. Domahidi, and M. Morari, "A model predictive control scheme with torque ripple mitigation for permanent magnet motors," in *Proc. 35th Annu. Conf. IEEE Ind. Electron.*, Nov. 2009, pp. 2943–2948. doi: 10.1109/IECON.2009.5415385.

[22] Z. Hu and K. Hameyer, "A method of constraint handling for speed-controlled induction machines," *IEEE Trans. Ind. Electron.*, vol. 63, no. 7, pp. 4016–4072, Jul. 2016. doi: 10.1109/TIE.2016.2532843.

[23] S. C. Carpiuc and C. Lazar, "Fast real-time constrained predictive current control in permanent magnet synchronous machine-based automotive traction drives," *IEEE Trans. Transport. Electrific.*, vol. 1, no. 4, pp. 326–335, Dec. 2015.

[24] T.-S. Kwon, M.-H. Shin, and D.-S. Hyun, "Speed sensorless stator flux-oriented control of induction motor in the field weakening region using Luenberger observer," *IEEE Trans. Power Electron.*, vol. 20, no. 4, pp. 864–869, Jul. 2005.

[25] F. Auger, M. Hilairet, J. M. Guerrero, E. Monmasson, T. Orlowska-Kowalska, and S. Katsura, "Industrial applications of the Kalman filter: A review," *IEEE Trans. Ind. Electron.*, vol. 60, no. 12, pp. 5458–5471, 2013.

[26] S. Bolognani, L. Tubiana, and M. Zigliotto, "Extended Kalman filter tuning in sensorless PMSM drives," *IEEE Trans. Ind. Appl.*, vol. 39, no. 6, pp. 1741–1747, Nov. 2003.

[27] P. Tøndel, T. A. Johansen, and A. Bemporad, "An algorithm for multi-parametric quadratic programming and explicit MPC solutions," *Automatica*, vol. 39, no. 3, pp. 489–497, 2003.

[28] P. Tøndel, T. A. Johansen, and A. Bemporad, "Evaluation of piecewise affine control via binary search tree," *Automatica*, vol. 39, no. 5, pp. 945–950, 2003.

[29] M. Herceg, M. Kvasnica, C. N. Jones, and M. Morari, "Multi-parametric toolbox 3.0," in *Proc. Eur. Control Conf.*, Jul. 2013 pp. 502–510. [Online]. Available: http://control.ee.ethz.ch/ mpt

[30] T.-J. Kweon and D.-S. Hyun, "High-performance speed control of electric machine using low-precision shaft encoder," *IEEE Trans. Power Electron.*, vol. 14, no. 5, pp. 838–849, Sep. 1999.

[31] J. Láfberg, "YALMIP: A toolbox for modeling and optimization in MATLAB," in *Proc. IEEE Int. Symp. Comput. Aided Control Syst.*, Sep. 2004 pp. 284–289, [Online]. Available: http://control.ee.ethz.ch/?joloef/yalmip.php

[32] S. Morimoto, M. Sanada, and Y. Takeda, "Wide-speed operation of interior permanent magnet synchronous motors with high-performance current regulator," *IEEE Trans. Ind. Appl.*, vol. 30, no. 4, pp. 920–926, Jul. 1994.

CHENGYU JIA was born in Heilongjiang, China, in 1983. He received the B.S. degree in electronic information engineering from Northeast Agricultural University, Harbin, China, in 2007, and the M.S. degree in power electronics from the Harbin University of Science and Technology (HUST), Harbin, China, in 2010, where he is currently pursuing the Ph.D. degree. His research interests include MPC and optimization, and optimal control of IPMSM.

XUDONG WANG was born in Heilongjiang, China, in 1958. He received the B.S. and M.S. degrees in electrical and electronic technology from the Harbin Institute of Electrical Engineering, Harbin, China, in 1982 and 1987, respectively, and the Ph.D. degree in mechatronic engineering from the Harbin Institute of Technology, Harbin, in 2000.

Since 1995, he has been a Professor with the Department of Electrical Engineering, Harbin University of Science and Technology (HUST). He holds more than ten National patents. He is a member of the Standing Director of the China Electrotechnical Society Power Electronics Committee. His awards and honors include provincial-level scientific and technological progress awards. His research interests include electrical machines design and drives, power electronics, and automotive electric traction drives.

YAFEI LIANG received the B.S. degree in electronics engineering from the University of Central Lancashire, U.K., in 2006, and the M.S. degree in control systems from Imperial College London, U.K., in 2008. From 2008 to 2018, he was an engineering Team Leader working in the field of powertrain systems and controls. His main research interests include new energy vehicles powertrain system, electrical machines drives. He honors the Beijing Nova Program 2013 Award.

KAI ZHOU received the B.S. degree in communication engineering from Qiqihar University, Qiqihar, China, in 2006, the M.S. degree in electrical engineering from the Harbin University of Science and Technology (HUST), Harbin, China, in 2009, and the Ph.D. degree in electrical engineering from HUST, in 2012, where he was appointed as an Associate Professor, from 2013 to 2018. His research interests include automotive electronics, motor control and test technology, and new energy vehicles.